Numerical modelling and field experimental validation of the axial load transfer on the drill-strings in deviated wells

Yuchun Kuang[a], Wei Lin[a,b,*], Yang Liu[b], Qin Wang[c], Jianzhong Zhang[d]

[a]*School of Mechatronic Engineering, Southwest Petroleum University, Chengdu, 610500, China*
[b]*College of Engineering, Mathematics and Physical Sciences, University of Exeter, North Park Road, Exeter, EX4 4QF, UK*
[c]*Chengdu iDrill Energy Technology Co. Ltd., Chengdu, 610500, China*
[d]*Drilling and Production Technology Research Institute of Jidong Oilfield, Petrochina, Tangshan, 063000, China*

Abstract

This paper studies the axial load transfer along the drill-strings in deviated wells by developing a finite element model based on the Euler beam theory and the augmentation Lagrangian contact algorithms. The model can simulate the entire drill-strings showing nonlinear contact model between drill-strings and casing. Special attention is given to the axial load loss, the pipe-casing contact force distribution and the slender pipe deformation. The efficacy of the proposed model is validated experimentally using a packer releasing procedure. Various drill-string factors, such as deviation angle, dogleg severity, hook load magnitude and buckling configurations, are considered for evaluating the efficiency of axial load transfer. Our analysis shows that the dogleg severity has a significant influence on the transfer, and the helical buckling of the drill-strings due to excessive loading could make it worse. This study provides a theoretical understanding of the variation of the contact force and the axial load transfer for the drill-strings in deviated wells. It can be used to better understand the working condition of downhole and guide field drilling.

Keywords: drill-string; axial load transfer; contact force; buckling; deviated well

1. Introduction

The aim of deviated well drilling as shown in Fig. 1 is to keep a well in a reservoir for a longer distance and maximise its productivity (Aadnoy and Andersen, 1998). One of the major challenges of deviated well drilling is to manage the mechanical loads on the drill-strings, namely, the so-called axial load transfer. In the phase of well development, effective weight-on-bit (WOB) is significant to keep drilling at a rate of penetration. In order to achieve this, the axial loads on the drill-strings and well trajectory should be optimised. But in the drilling operation of deviated wells, excessive drag makes the efficiency of axial load transfer low. Here, drag is the incremental force required for lifting up or down of the drill-strings. Large drag is problematic in the deviated wells due to the increased well horizontal length, especially for the less thick and stiff drill-strings. So, this problem has attracted great attention in the past few years, see e.g. (Duman et al., 2003; Menand et al., 2009; Miska et al., 1996; Omojuwa et al., 2012; Zhu et al., 2015).

In order to improve the efficiency of axial load transfer, a great deal of theoretical and experimental works focusing on drill-strings' drag force have been carried out (Mirhajmohammadabadi et al., 2010). In the conventional approach (Johancsik et al., 1984), drill-strings were considered as a cable under tension,

*Corresponding author
Email addresses: swpikyc@126.com (Yuchun Kuang), weilin_swpu@hotmail.com (Wei Lin), y.liu2@exeter.ac.uk (Yang Liu), wqhf-wang@163.com (Qin Wang), zcy_zhangjzh@petrochina.com.cn (Jianzhong Zhang)

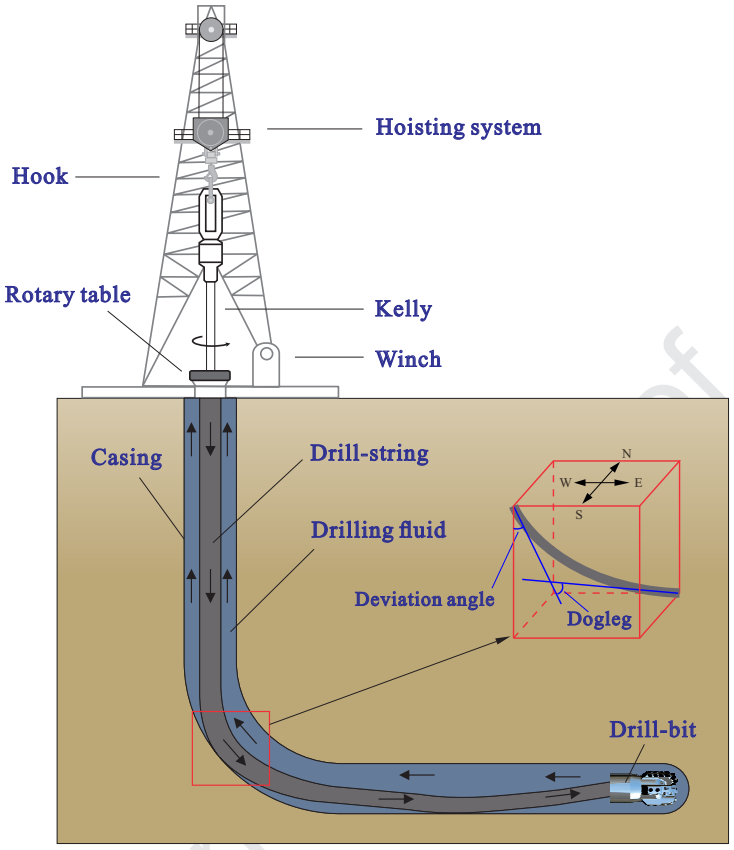

Figure 1: (Colour online) Schematics of a horizontal well drilling rig. Deviation angle is the angle between the tangential direction of well trajectory and the vertical direction. Dogleg severity is a measure of the amount of change in the direction of a borehole, usually expressed in degrees per 30 m length.

the so-called soft-string model, which can be mathematically expressed as

$$\begin{cases} F_n &= \sqrt{[(F_t \Delta\alpha \sin\theta)^2 + (F_t \Delta\theta + W \sin\theta)^2]} \\ \Delta F_t &= W\cos\theta \pm \mu F_n \end{cases} \tag{1}$$

where F_n and ΔF_t are the magnitudes of the normal force and tension increment, respectively. According to the analytical models studied in Aadnoy and Andersen (1998); Brett et al. (1987); Miska et al. (1996); Sheppard et al. (1987), well trajectory can be considered in straight, arc, and inclined straight sections. Considering the limitation of the soft-string model, Ho (Ho, 1988) proposed a stiff-string model to study the influence of string stiffness on string-borehole contacts. Opeyemi and Pham (Adewuya and Pham, 1998) developed a novel torque and drag analysis approach for well planning and drill-string design. Based on the Euler beam theory, many researchers (Aadnoy and Andersen, 1998; Maehs et al., 2010; Miska et al., 1996) investigated the possibility of pipe buckling under the condition of drill-string compression. With the development of finite element method, numerical methods, e.g. (Kuang et al., 2016; Meier et al., 2014; Omojuwa et al., 2012; Tikhonov and Safronov, 2008), were proposed to solve drill-string dynamics for complex trajectory. In (Cebeci and Kök, 2019; Hill and Chandler, 1998; Huang and Gao, 2019; Mitchell and Miska, 2006; Qin et al., 2019), numerical models were developed to study drill-string buckling and axial load transfer in different buckling configurations. Lubinski (Lubinski, 1950) analysed the stress and deformation of a buckled drill-string, and the helical buckling of tubing sealed in packers (Lubinski and Althouse, 1962) based on the theory of elastic stability. According to these works, a series of models were established. The buckling equation and natural boundary conditions were derived with the aid of calculus of variations by Gao and Miska (2010). They found that the pipe can be consid-

ered as if its dimensionless length is greater than 5π, and thus, the effect of boundary conditions at both end can be ignored. Based on the experimental study, Duman et al. (2003) found that the tool joints increase the critical load of the helical buckling about 20%, and drill string rotation was benefit for the axial load transfer even it exceeds the buckling criteria load (Menand et al., 2009). Mitchell (1996) and Miller et al. (2015) studied the criteria of buckling load and axial load transfer by considering various friction coefficients, pipe connectors, and annular clearances. In addition. Kapitaniak et al. (2015, 2016, 2018a,b) proposed a finite element model for the buckled configuration of a drill-string, which allows them to observe the effect of winding and unwinding of the helical deformation during complex vibration. In these cases, because of the simplification of actual well trajectory and neglect of the contact model, it is not possible to predict axial load transfer. Therefore, the actual well trajectory and contact model should be performed to analyse axial load transfer for entire drill-strings.

The present work will study a finite element model of the drill-strings interacting with borehole which takes into account the actual well trajectory during the procedure of packer releasing by using ANSYS/APDL. Experimental verification will be carried out in an oil field, which has an accurate measurement of the axial load at the different locations of the well. A comparison of the axial load transfer during a packer releasing procedure between the field experimental and the simulation data yields a good agreement. Based on the proposed model, the influences of the deviation angle and the overall angle change rate will be studied, and the results manifest that the change rate of overall angle has a significant influence on the transfer efficiency of the axial load and the distribution of the contact force. In addition, the investigation on the buckling of the horizontal drill-strings will be carried out at different deformation configurations. Our results show that the transfer efficiency is approximately linear with the increase of the axial displacement, when the configuration of the drill-strings is straight and sinusoidal, while it is fluctuated dramatically when the configuration is helical. The main contributions of the current work are (1) a FEM is proposed by taking into account the actual well trajectory and by studying the contact force distribution; (2) the overall angle change rate has a significant influence on the axial load transfer; (3) the axial load transfer is sensitive to the buckling configurations of the drill-strings.

The rest of the paper is organized as follows. In Section 2, the FEM and its corresponding theory will be studied. The effectiveness of the proposed FEM will be validated using field data in Section 3. In Section 4, the influences of parametric sensitivity and buckling configurations in horizontal well on the axial load transfer will be investigated. Finally, some concluding remarks are drawn in Section 5.

2. Finite element model

Based on the finite element method, the nonlinear model of the entire drill-string and casing/wellbore is developed by using the ANSYS/APDL platform. Input parameters and data, including the well trajectory, drill-string physical and geometrical parameters and tripping parameters, are considered. The procedure of the simulation study is shown in Fig. 2. For the entire drill-string model, it is easy to simplify the clear boundary at the wellhead. Thus, the proposed FEM can be used to simulate the actual state of the axial force transfer for the entire drill-strings. However, due to the slenderness ratio and the lengthy drill-strings, especially when considering the contact between the drill-strings and the casing, the number of the elements in the FEM is numerous, and the computation of the nonlinear model is time-consuming so inefficient. Therefore, it needs to find appropriate level of details in modeling in order to gain a balance between accurate model and fast computation. To achieve this balance, the following hypothesis must be satisfied:

(a) Only small deformation is considered;
(b) The existence and influence of pipe connectors are neglected;
(c) Casing wall and well bore are rigid;
(d) Viscous force on the drill pipe due to the drilling mud is neglected.

2.1. Element description and string-casing contact model

The Euler beam element shown in Fig. 3 is used to model the drill-string by taking into account tension-compression, torsion, and bending. The element has six degrees of freedom at each node, namely

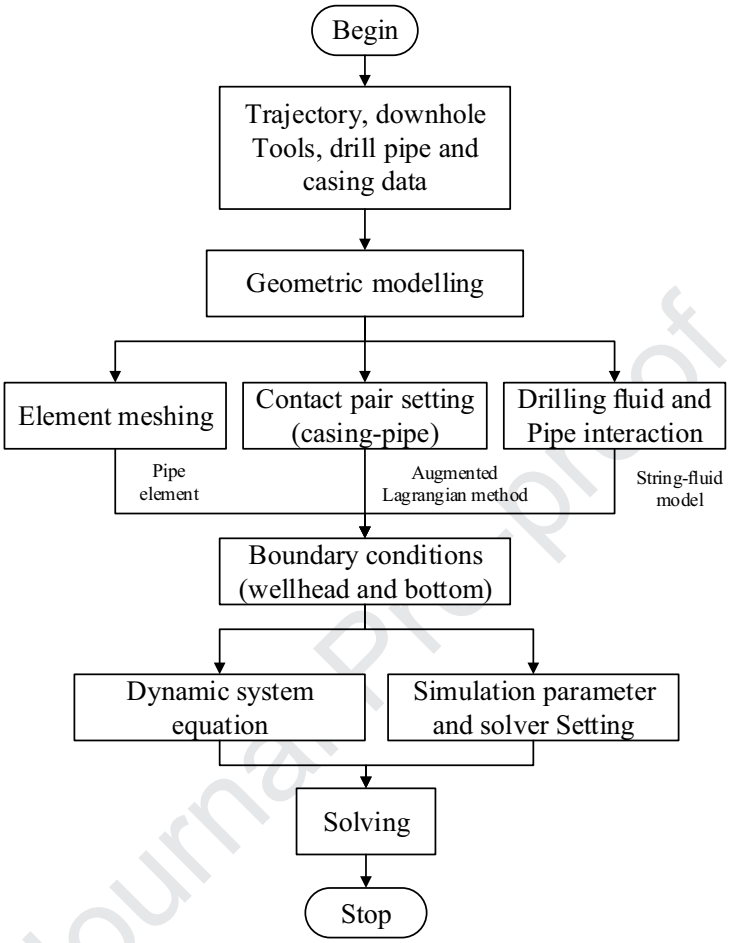

Figure 2: The flowchart of the simulation study of the drill-strings.

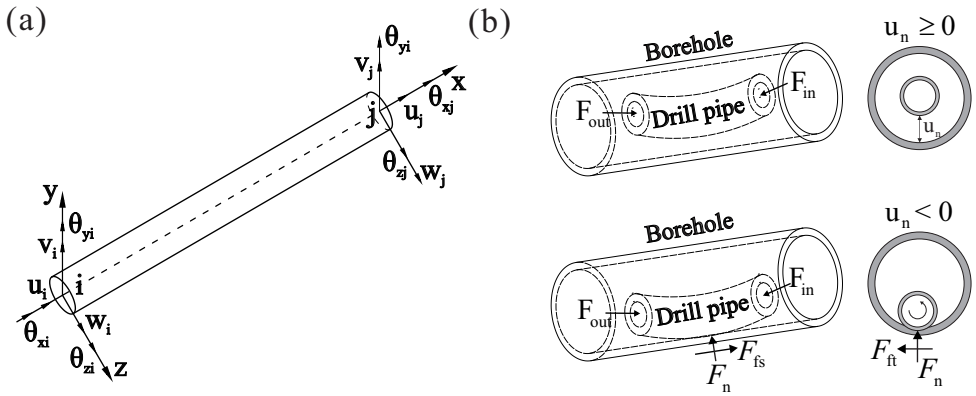

Figure 3: (a) Euler beam element with two nodes, and each node has three rotational and three translational degrees of freedom. (b) Two types of the contact between the drill-string and the well bore. Right panels show the cross-section of the contact. F is the axial interactive force between each element, F_{n} is the contact force between the drill pipe and the casing, F_{fs} is the translational friction force, and F_{ft} is the rotational friction force between the drill pipe and the casing.

the translations in the nodal x, y, and z directions and the rotations about the nodal x, y, and z axes. The loads applied on this element include the hydrodynamic and buoyant effects of the drilling mud and the element mass including the added mass of the drilling mud and the pipe internals. For analysing the drill-string dynamics, the nodal displacement, which can be written as

$$\{\delta_e\} = \{u_i, v_i, w_i, \theta_{xi}, \theta_{yi}, \theta_{zi}, u_j, v_j, w_j, \theta_{xj}, \theta_{yj}, \theta_{zj}\}, \tag{2}$$

is changing with the element force, where u_i, v_i, and w_i represent the displacements of node i in x, y, and z direction, respectively, θ_{xi}, θ_{yi}, and θ_{zi} are the angular displacements about x, y, and z axes, respectively, and the variables with the subscript j represent the corresponding displacements of node j. Then the shape function (Shooshtari and Khajavi, 2010) can be expressed as

$$[N] = \begin{bmatrix} N_1 & 0 & 0 & 0 & 0 & 0 & N_2 & 0 & 0 & 0 & 0 & 0 \\ 0 & N_2 & 0 & 0 & 0 & N_4 & 0 & N_5 & 0 & 0 & 0 & N_6 \\ 0 & 0 & N_3 & 0 & -N_4 & 0 & 0 & 0 & N_5 & 0 & -N_6 & 0 \\ 0 & 0 & 0 & N_1 & 0 & 0 & 0 & 0 & 0 & N_2 & 0 & 0 \end{bmatrix}, \tag{3}$$

where $N_1 = (1-s)/2$, $N_2 = (1+s)/2$, $N_3 = 1/s - s(3-s^2)/4$, $N_4 = L(1-s^2)(1-s)/8$, $N_5 = 1/2 + s(3-s^2)/4$, $N_6 = L(1-s^2)(1+s)/8$. L is the element length, $s = (2q/L - 1) \in [-1, 1]$, on node i ($q = 0$), $s = -1$, on node j ($q = L$), $s = 1$, q is the node coordinate in the nodal coordinate system.

For the nonlinear contact between the drill-string and the casing (borehole), it is highly nonlinear contact and friction. The augmented Lagrange method (Hestenes, 1969; Simo and Laursen, 1992), which is less sensitive to the magnitude of the contact stiffness, was used in this work. This method consists of a special combination of the penalty and Lagrange multiplier method, which converges to the solution for a finite penalty coefficient and provides an unconstrained minimization problem with a smooth functional. In the FEM, the contact force can be written as

$$F_n = \begin{cases} 0 & if\ u_n \geq 0, \\ k_n u_n + \lambda & if\ u_n < 0, \end{cases} \tag{4}$$

where k_n is the contact stiffness, u_n is the penetration of drill-string into the casing, and λ is the extra term determined by the penetration tolerance ϵ, which can be updated as

$$\lambda_{i+1} = \begin{cases} \lambda_i + K_n u_n & if\ |u_n| \geq \epsilon, \\ \lambda_i & if\ |u_n| < \epsilon. \end{cases} \tag{5}$$

The augmented Lagrange formulation (Yastrebov, 2013) can be written as

$$\mathcal{L}^a(x, \lambda_i) = \mathcal{L}(x, \lambda_i) + \frac{1}{2}\epsilon g(x)^2 \tag{6}$$

This method is a constrained minimization problems, and the augmented Lagrangian algorithm for frictional contact is presented in Table 1, where the parameters in the table can be found from Simo and Laursen (1992).

2.2. Fluid-string interaction

The fluid inside the hollow pipe induces inertial force on the drilling assembly, which was implemented by adding the extra mass in our model. The effects of the fluid between the drill-string and the casing are characterized as inertial and drag forces. Since the influence of the fluid flow in axial direction is neglected, the inertial force, i.e. the hydrodynamic load, can be calculated using the Morison equation (Wheeler, 1970) as

$$\{F/L\} = \rho_w A\{\ddot{v}\} + C_a \rho_w A\{\ddot{v} - \ddot{u}\} + \tfrac{1}{2}\rho_w C_d D_e |\{\dot{v} - \dot{u}\}|\{\dot{v} - \dot{u}\}, \tag{7}$$

where $\{F/L\}$ is the vector of loads per-unit length due to hydrodynamic effects, ρ_w is the water density, A is the cross-section area, $\dot{v}$ and $\ddot{v}$ represent the velocity and the acceleration of the drilling mud, $\dot{u}$ and

Table 1: The augmented Lagrangian algorithm for frictional contact (Simo and Laursen, 1992).

1. Initialization
   set $\lambda^0 = \langle \lambda_N + \epsilon_N g \rangle$ from last time step
   $\Delta\lambda_T^{(k)} = 0$
   $\Gamma_{stick}^{(0)} = \Gamma$
   $k = 0$
2. Solving (using a nonlinear solution strategy) for $u_{n+1}^{(k)}$
   $G(u_{n+1}^k, \delta u) + \int_\Gamma [\left\langle \lambda_N^{(k)} + \epsilon_N g(u_{n+1}^{(k)}) \right\rangle \delta u \cdot n + t_T(u_{n+1}^{(k)}) \cdot \delta u_T] d\Gamma = 0$
   where
   $$t_T(u_{n+1}^{(k)}) = \begin{cases} t_{T_n} + \Delta\lambda_T^{(k)} + \epsilon_T \Delta u_T^{(k)} & if \quad x \in \Gamma_{stick}^{(k)} \\ \Delta\lambda_T^{(k)} + t_{T_n} & otherwise \end{cases}$$
3. Check for constraint satisfaction.
   IF $g(u_{n+1}^k) \leq TOL1$ for all $x \in \Gamma$ AND $\|u_{T_{n+1}} - u_{T_n}\| \leq TOL2$
   for all $x \in \Gamma$ such that $\|t_T\| < \mu \left\langle \epsilon_N g + \lambda_N^{(k)} \right\rangle$ AND
   $\|t_T\| \leqslant (1 + TOL3)\mu \left\langle \epsilon_N g + \lambda_N^{(k)} \right\rangle$ for all $x \in \Gamma$ THEN
   Converge, EXIT.
   ELSE
   Augment and update Γ_{stick} (for all $x \in \Gamma$):
   $\lambda_N^{k+1} = \left\langle \lambda_N^{(k)} + \epsilon_N g(u_{n+1}^{(k)}) \right\rangle$
   IF $(\|t_{T_n} + \Delta\lambda_T^{(k)} + \epsilon_T \Delta u_T^{(k)}\| \leq \mu\lambda_N^{(k+1)})$ THEN
   $\Delta\lambda_T^{(k+1)} = \Delta\lambda_T^{(k)} + \epsilon_T \Delta u_T^{(k)}$,
   $x \in \Gamma_{stcik}^{(k+1)}$
   ELSE
   $\Delta\lambda_T^{(k+1)} = \frac{t_{T_n} + \Delta\lambda_T^{(k)} = \epsilon_T \Delta u_T^{(k)}}{\|t_{T_n} + \Delta\lambda_T^{(k)} + \epsilon_T \Delta u_T^{(k)}\|} \mu\lambda_N^{(k+1)} - t_{T_n}$
   $x \notin \Gamma_{stick}^{(k+1)}$
   $k \leftarrow k + 1$
   GO TO 2.
   ENDIF

$\ddot{u}$ represent the velocity and the acceleration of the drill-string, C_a and C_d are the added mass and drag coefficients, respectively, and D_e indicates the outer diameter of the drill-string.

2.3. Dynamic theory

To study the axial load transfer, most of the previous works have focused on the motion of the drill-strings in static state and the derivation of its analytical solution after the well trajectory was simplified to straight, build-up and incline-straight sections in a two-dimensional plane only. Limitation of these works is that the dynamical behaviour and the local geometrical characteristics of the well trajectory, such as dogleg severity, which are crucial for evaluating the efficiency of axial load transfer, were not included in the model. So, a comprehensive model of axial load transfer should always take these complex factors into account. According to the Hamilton principle (Leigh and Kunz, 2007; Thompson et al., 2012), the kinetic energy, the potential energy and the work done by the non-potential forces, must satisfy the following energy conservation equation,

$$\delta \int_{\Delta t} (T - V) + \int_{\Delta t} \delta W = 0, \tag{8}$$

where T is the kinetic energy, V is the potential energy, and W is the work done by the non-potential forces. For a continuous system, T, V, and W can be expressed by using the displacement variables (u, θ) and the velocity variables $(\dot{u}, \dot{\theta})$. For our proposed model, T, V, and W can be obtained via the integration method by using the shape function (3). Then by substituting U_i into Eq. (8), we can obtain the following non-potential equation,

$$\int_{\Delta t} \Big[-\frac{d}{dt}\Big(\frac{\partial L}{\partial \dot{U}_i}\Big) + \frac{\partial L}{\partial U_i} + F_i \Big] \delta U_i = 0, \tag{9}$$

where $L = T - V$ is the Lagrange function, which can be expressed as $L = T - V$. Since δU_i is an arbitrary variable, Eq. (9) can be rewritten as (Chen et al., 2018; Zhu et al., 2015)

$$-\frac{d}{dt}\Big(\frac{\partial L}{\partial \dot{U}_i}\Big) + \frac{\partial L}{\partial U_i} + F_i = 0, \tag{10}$$

Substituting $L = T - V$ into Eq. (10), it gives

$$\frac{d}{dt}\Big(\frac{\partial T}{\partial \dot{U}_i}\Big) - \frac{\partial T}{\partial U_i} - \frac{\partial V}{\partial U_i} = F_i. \tag{11}$$

Considering collecting all the elements together, the dynamic equation of the drill-strings can be written as

$$M\ddot{u} + C\dot{u} + Ku = F, \tag{12}$$

where M, C and K are the mass, the damping and the stiffness matrices, respectively. $\ddot{u}$, $\dot{u}$, and u represent the acceleration, the velocity, and the displacement of the rotation and the translation of the node, respectively. F represents the external generalized forces.

In the present work, the transfer efficiency of the axial load can be calculated as

$$\beta = \big|F^{\text{in}} - F^{\text{out}}\big| / \Delta L, \tag{13}$$

where β donates the axial load loss per 100 m. F^{in} and F^{out} are the input and the output of the axial force, respectively, and ΔL is the length of the considered string. When $\beta = 0$, there is no axial load loss, and the larger β, the more axial force loses.

3. Model validation

A packer releasing process was measured in the field by using five dynamical measurement subs in a down-flow well. This practical well is a deviated well with the 'straight-buildup-straight' section in Eastern China, which has a measured depth of over 3600 m as shown in Fig. 4(a). With the maximal deviation angle of 45 degrees, the true vertical depth and the horizontal length are 2856 m and 2000 m, respectively. The starting point of the build-up section locates at 300 m, and the incline straight section begins at 800 m. According to the logging data, it has the maximum overall angle of 3.8 degrees per 30 m near 2800 m and the overall angle change rate is presented in Fig. 4(b).

3.1. Field experimental set-up and procedure

In order to study the change rule for the axial load in directional well, five measurement subs, placed at the well-head (10 m), the kick off point (300 m), the starting point of the incline straight section (800 m), the point at the incline straight section (1000 m), and the point near the packer (3000 m), were employed to record the axial load, torque, and internal pressure. All the subs record field data at every four seconds, and only the axial load data was used in this paper. An overview schematic of the drill pipes and the measurement subs is presented in Fig. 5, where all of the corresponding parameters are given in Table 2. During the process of packer releasing, pulling out and tripping in were carried out alternately to keep the drill pipe safe.

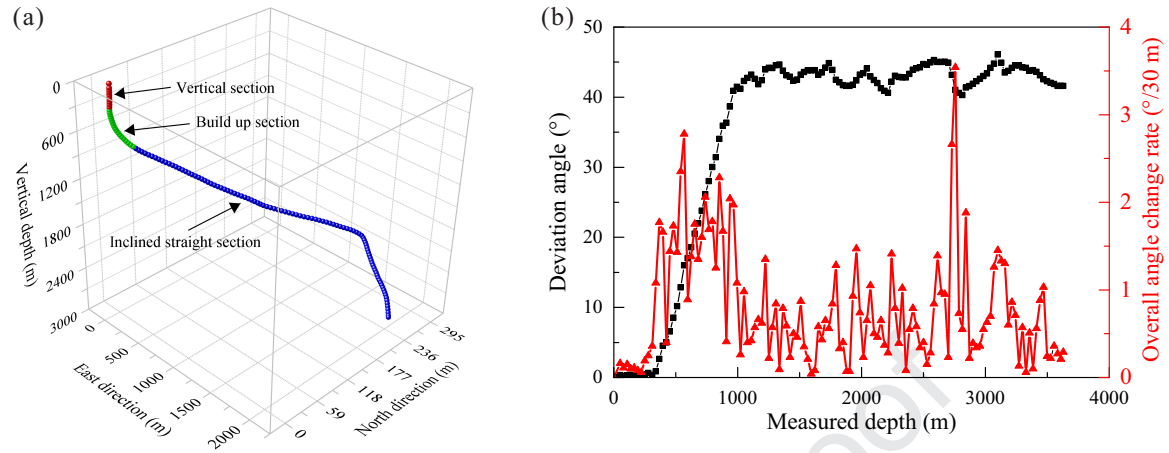

Figure 4: (Colour online) (a) Well trajectory, and (b) the deviation angle and the change rate of overall angle.

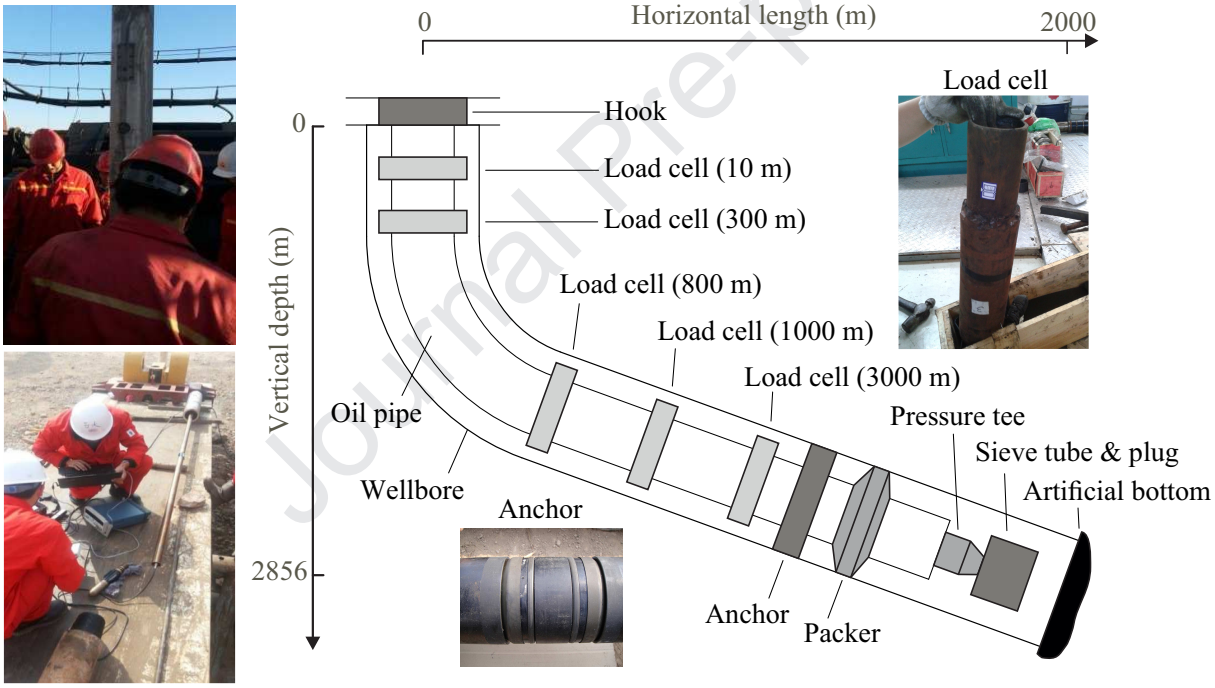

Figure 5: (Colour online) Schematic of the measurement subs and the drill pipe components.

Table 2: Physical parameters of the drill pipe in the test well

Parameters	Value
Borehole diameter	121 mm
Pipe external diameter	73 mm
Pipe internal diameter	62 mm
Pipe mass density	7800 kg/m^3
Pipe Young's modulus	2×10^{11} Pa
Pipe-casing friction coefficient	0.3
Fluid mass density	1000 kg/m^3

3.2. Field testing results

According to the measurement data recorded in the driller system, the hook load has a significant change from 363 kN to 168 kN at 200 s indicating that the packer releasing has completed. The axial load data from the five measurement subs was collected and presented in Fig. 6, where the segments A, C and E show the procedure of pulling out, and the segments B and D show the change of the axial load during the procedure of tripping in. As can be seen from the figure, in segment A, the axial loads measured by the subs increase linearly as the measurement goes deeper. At about 50 s, in segment B, driller decreased the hook load to prevent the drill pipes from damage. Both axial loads measured at 10 m and 300 m were reduced, while the axial loads measured at 800 m, 1000 m, and 3000 m were kept the same. Thereafter, driller pulled out the drill pipes in segment C, where the increases of the axial loads at 10 m and 300 m were much greater than the increases at 800 m, 1000 m and 3000 m. Segment D and E repeated the same procedures as the segments B and C. As the axial force increased gradually, the packer releasing occurred in segment F when the axial load measured at 3000 m achieved 123 kN, and the axial load measured at 10 m at that moment was 365 kN.

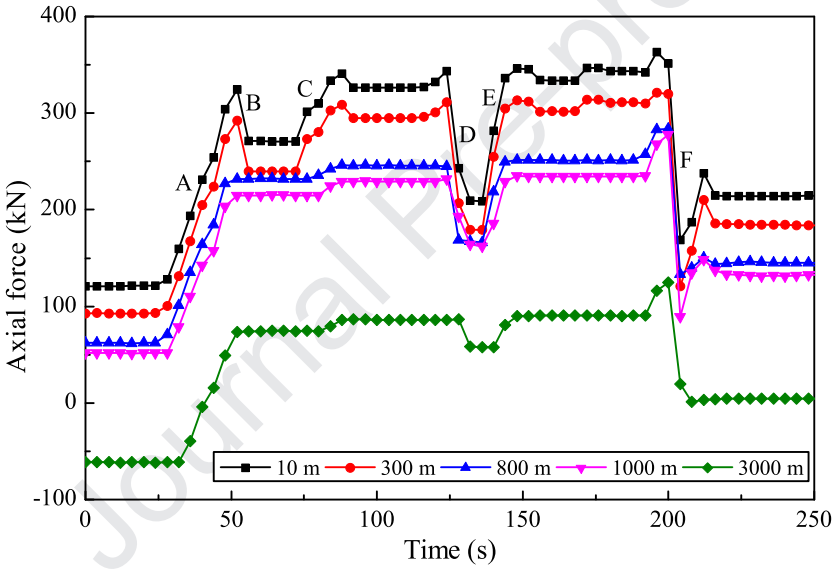

Figure 6: (Colour online) Field data of the axial load during a packer releasing process at the measured depth: 10 m, 300 m, 800 m, 1000 m, and 3000 m, where the segments A, C, E, and F indicate the procedure of pulling out, and the segments B and D show the procedure of tripping in.

3.3. Model analysis and validation

Numerical simulation based on the proposed FEM was carried out by using the physical parameters of the test well given in Table 2. Since the entire well bore is steel-oil casing, we used the general steel-steel friction coefficient which is 0.2 in our simulation. The boundary at the top of the drill pipes was restricted to the axial direction only, so the hook load can be recorded when the pipe was tripped-in to different measured depths. Fig. 7 compares the hook loads between our simulation and field testing results during the tripping-in procedure which shows a good agreement.

In order to simulate the packer releasing procedure, the node at the bottom was fixed when the axial force was less than the releasing force 123 kN, and the axial displacement was applied to the node at the wellhead once the axial force is greater than this releasing force. Fig. 8 illustrates the simulation results at the releasing moment. As shown in Fig. 8(a), the width of the colour map, which is perpendicular to the element axial direction, is used to indicate the magnitude of the axial load. Since the displacement step was set as 0.01 m, our simulation will stop if the axial load at the bottom is greater than the axial load for packer releasing. Our calculation shows that, once the axial load measured at 3000 m achieved

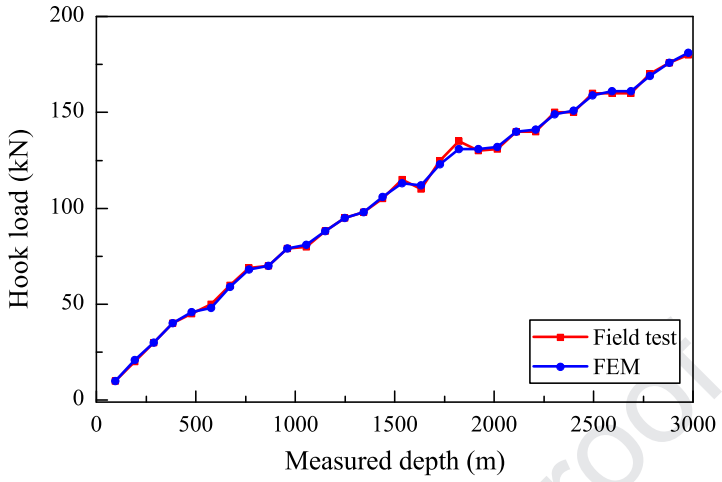

Figure 7: (Colour online) Hook loads during the tripping-in procedure.

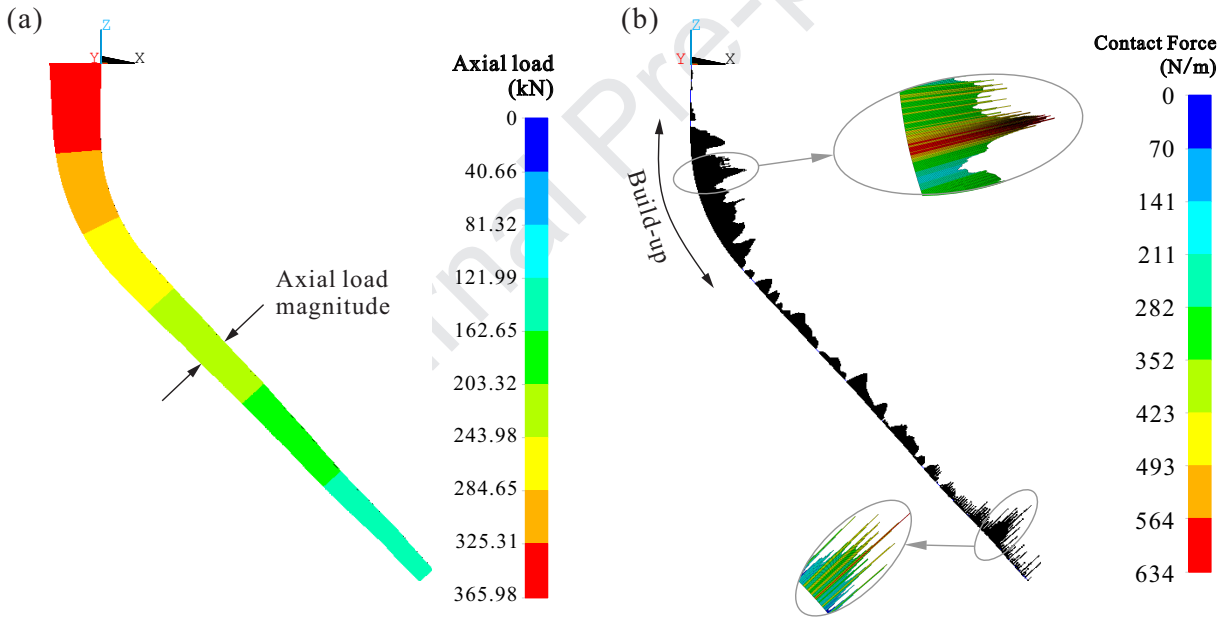

Figure 8: (Colour online) Packer releasing moment: (a) the axial loads of the entire drill pipes, and (b) the contact forces between the drill pipes and the casing. The width of the colour map which is perpendicular to the element axial direction represents the magnitude of the axial load.

122.8 kN, i.e. the releasing load, the axial load measured at 10 m was recorded at 364.6 kN. This result is consistent with our field testing observation presented in Fig. 6. On the other hand, the contact forces between the drill pipes and the casing are presented in Fig. 8(b). The contact forces recorded at the build-up section are much greater than the other two sections, and the forces in the middle of the build-up section are the greatest. Furthermore, a small segment near 2800 m has greater contact forces, since the angle of the dogleg in this segment is the greatest as indicated in Fig. 4(b).

The axial forces along the entire drill pipes subjected to the loading and unloading phases at different depths are shown in Fig. 9, where the maximum displacement applied to the wellhead was implemented at 2.5 m, 3.0 m, and 3.5 m. As shown in Fig. 9(a), the axial loads at 300 m are linear with the loads at 10 m, and the axial loads in the loading and unloading phases were kept the same. As presented in Fig. 5, the drill pipes at 10 m and 300 m are both in the vertical section, so their contact forces with the

casing are small. As can be seen from Fig. 9(b-d), the axial forces at 800 m, 1000 m, and 3000 m for the loading and unloading phases are different. With the increase of the axial load at 10 m, the loads in the loading phase (red arrows) are less than the ones in the unloading phase (green arrows).

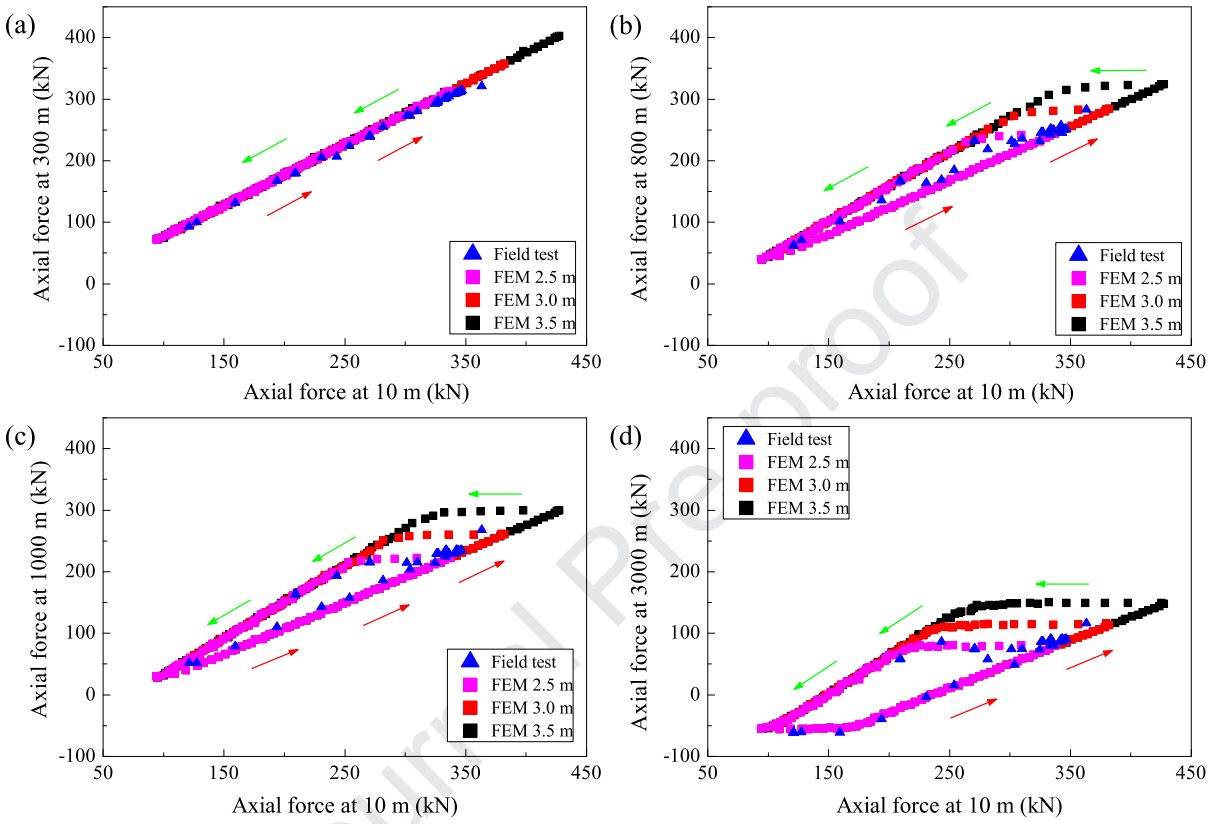

Figure 9: (Colour online) The comparison between the field testing and the simulation data is presented. Blue triangles represent field testing data, and black, red, and purple squares stand for the loading (pulling out) and unloading (tripping in) phases with the maximum displacement of 2.5 m, 3.0 m, and 3.5 m at the wellhead, respectively. Red and green arrows indicate the loading and unloading phases, respectively.

It is obvious that the distribution of the contact forces along the drill pipe has significant influence on the axial load transfer. Fig. 10 presents the contact forces along the drill pipes recorded in our FEM, which shows the maximum displacement of 3.5 m in both loading (Fig. 10(a)) and unloading (Fig. 10(b)) phases, where x-axis is the axial displacement, y-axis is the measured depth, the colour represents the magnitude of the contact force, and the yellow squares indicate the neutral points at where the axial load is zero. As can be seen from Fig. 10(a), when the axial displacement is greater than 0.8 m, the entire drill pipes are in extension, and the contact force increases as the axial displacement increases. In the build-up section, the contact forces are greater than the forces in the other two sections. At the measured depth of 2800 m, where the maximum overall angle change rate is encountered, larger contact forces were recorded again. Similar force distribution can be observed from the unloading phase as shown in Fig. 10(b). However, comparing the corners below the neutral points in both figures, when the pipes are in compression in loading phase, the contact force increases immediately, while in unloading phase, the contact force decreases rapidly.

Fig. 11 compares the contact forces of the loading (blue) and unloading (red) phases for different axial displacements. When the axial displacement is 0.05 m, the drill pipes below 1600 m are in compression, and the contact forces near the bottom fluctuate in both phases as indicated by the grey area in Fig. 11. As the axial displacement increases, the contact forces at the build-up section in loading phase become greater than the ones in the unloading phase. In addition, another important observation is that the contact forces have the same variation trend as the overall angle change rate varies.

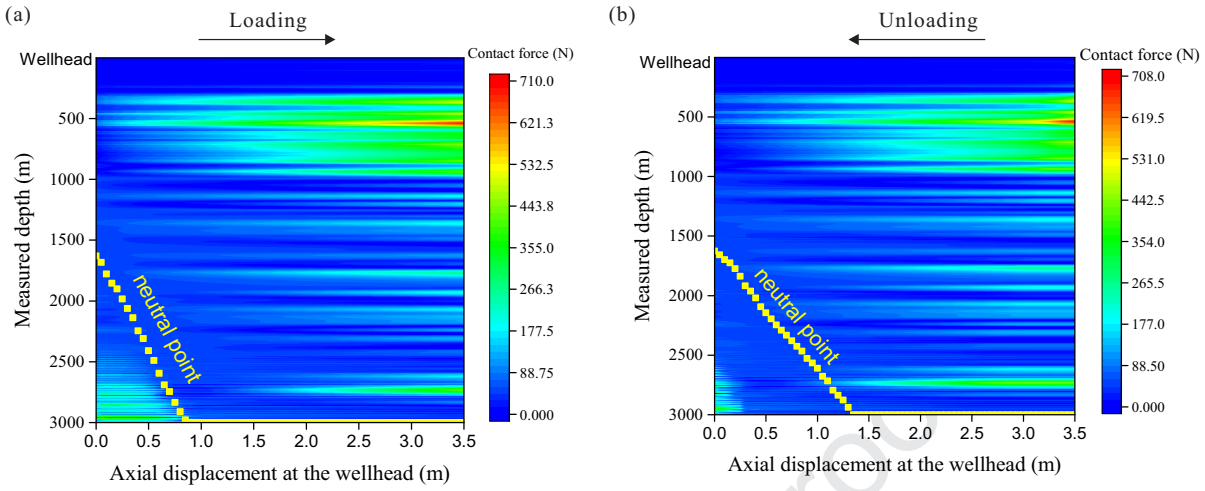

Figure 10: (Colour online) The map of the contact forces between the drill pipes and the casing calculated by using the model 12: (a) loading phase with the maximum displacement of 3.5 m, and the pipes are in extension after 0.8 m; (b) unloading phase with the axial displacement indicating partial pipes are in compression when the axial displacement is less than 1.3 m. Yellow squares represent the neutral points at where the axial load is zero.

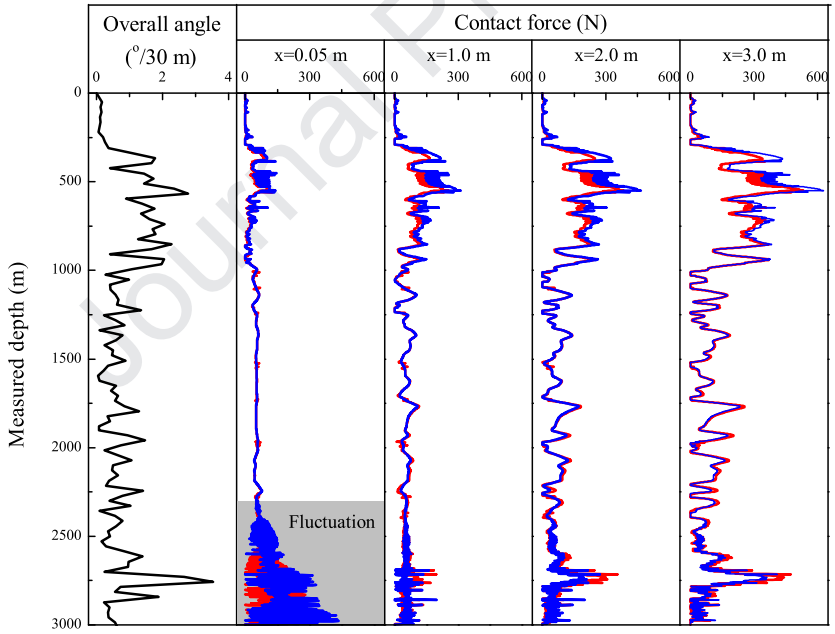

Figure 11: (Colour online) The contact forces of the entire drill-strings in the loading and the unloading phases with different axial displacements. Blue lines denote the contact forces in the loading process, and red lines indicate the contact forces in the unloading process.

4. Parametric analysis

This section studies the factors that may influence the axial load transfer in the build-up section and the buckling in horizontal section, such as deviation angle, overall angle change rate, tripping velocity, buckling configurations and drill-string components.

Four deviated well trajectories were modelled with the vertical length of 300 m, the inclined straight length of 1000 m, and the curvature radius of 500 m. Our calculations are shown in Fig. 12(a), where the

loss of axial load is plotted as a function of the hook load. It can be seen from the figure that, the losses of axial load for the four wells increase linearly as the hook load increases. When the deviation angle is 20°, it has the largest loss of the axial load. Although the pulling forces at the wellhead are the same, the contact forces for the deviation angle of 20° are larger than the other cases. The loss of the axial load for different overall angle change rates are presented in Fig. 12(b). It can be observed from the figure that the loss of axial load increases linearly with the change rate of the overall angle, and the change rate is more sensitive than the deviation angle. When the hook load is more than 250 kN, the loss increases significantly. When the change rate of the overall angle is 80° per 30 m, the loss of the axial load is the largest. It can prove that when the overall angle change rate is the same, the slope factor is consistent, as is shown in figure 12(a).

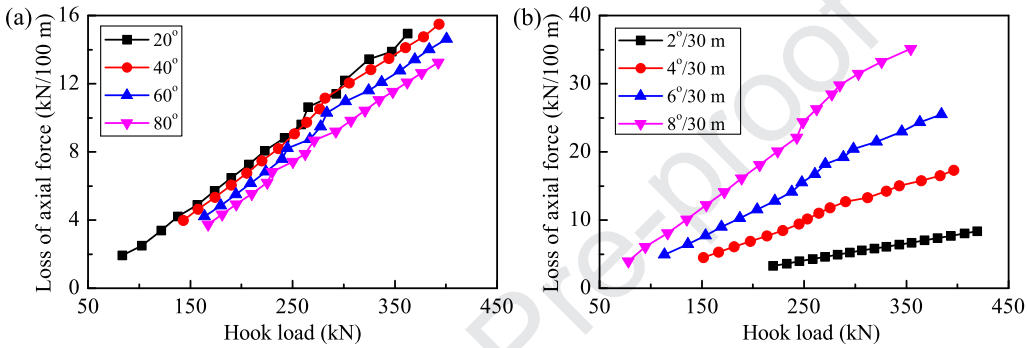

Figure 12: (Colour online) Axial load loss as a function of the hook load under (a) different deviation angles and (b) different overall angle change rates.

In field operation, the velocities of tripping in and pulling out have influence on the axial load transfer, particularly when the horizontal section is lengthy. Fig. 13 shows the axial loads calculated by using the proposed FEM for different pulling-out and tripping-in velocity configurations. It can be see from Fig. 13(a) that, the pulling-out force increases with the tripping velocity, and this increase is significant in the build-up section at the measured depth between 300 m and 1000 m. On the other hand, as shown in Fig. 13(b), the tripping velocity does not affect the axial load too much for tripping in operation.

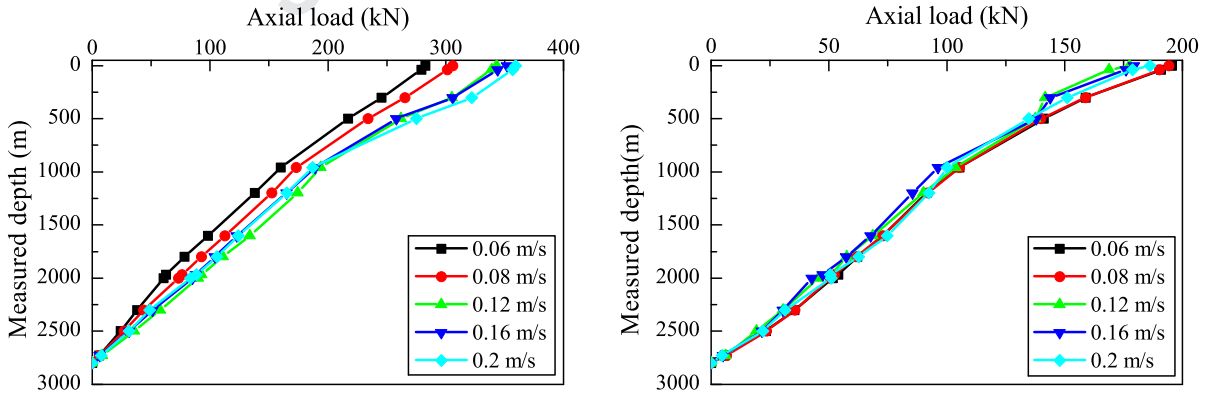

Figure 13: (Colour online) The axial load for (a) pulling-out and (b) tripping-in operations under different tripping velocities.

When the drill-strings are in compression, it could be in buckling due to excessive axial load, and this may significantly reduce the efficiency of the axial load transfer. Next, a 300 m long drill-strings with 73 mm outer diameter and 62 mm inner diameter was simulated in a horizontal well. The dead end was fixed, and the axial displacement was applied to the loading end of the drill-strings. Fig. 14 presents the buckling configurations of the drill-strings under different axial displacements. As can be seen from the

figure, when the axial displacement is 0.1 m, the drill-strings are straight. Sinusoidal and helical buckling configurations can be observed at the loading end when the axial displacement is increased to 0.11 m. As the axial displacement increases, such buckling is transferred to the dead end along the drill-strings. The coexistence of the straight, sinusoidal and helical buckling configurations on the drill-strings is kept until the axial displacement increases to 0.13 m. Thereafter, the entire drill-strings become buckling, and it is completely in helical buckling when the axial displacement is increased to 0.15 m.

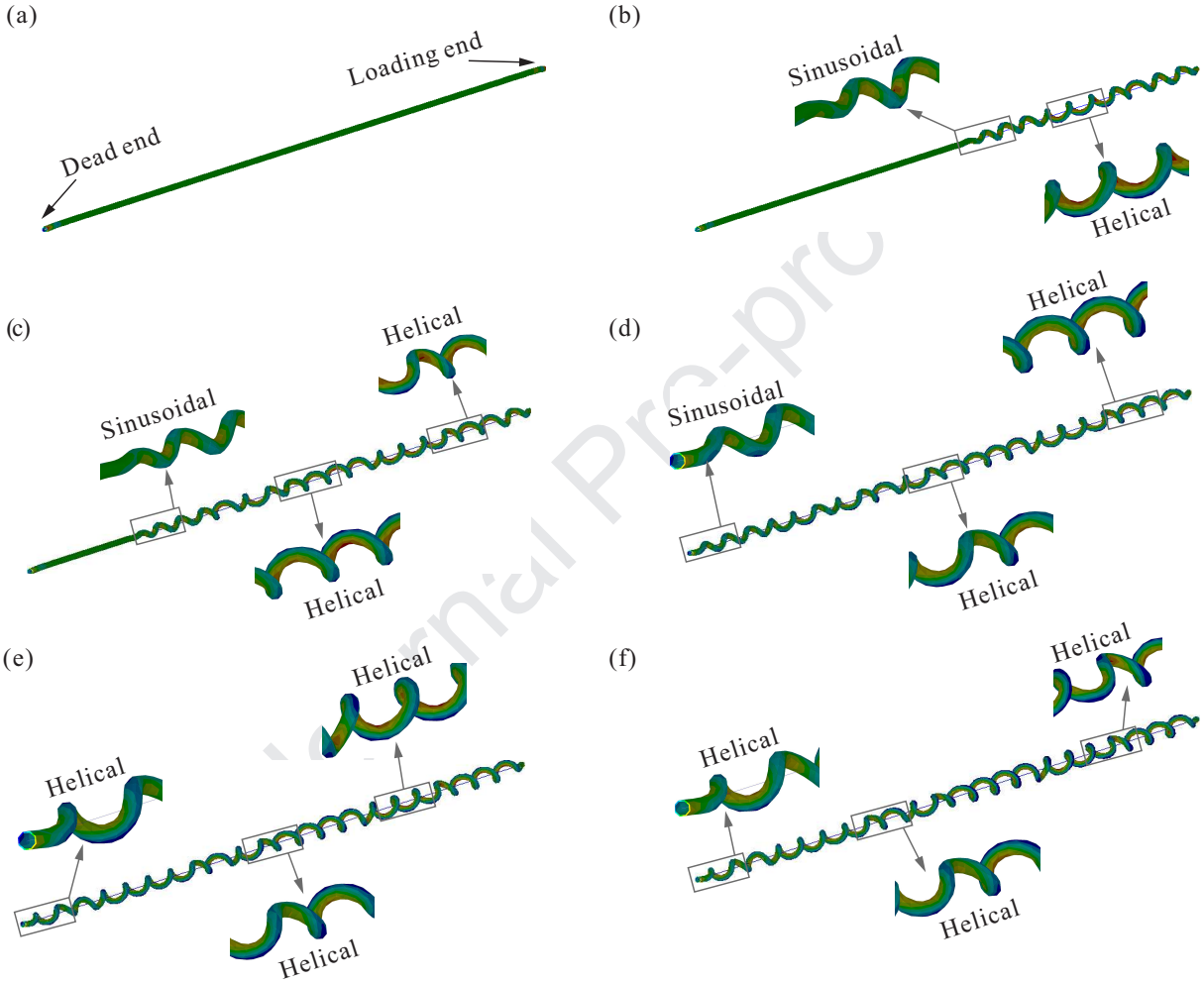

Figure 14: (Colour online) Drill-string configurations under different axial displacements: (a) $x = 0.1$ m; (b) $x = 0.11$ m; (c) $x = 0.12$ m; (d) $x = 0.13$ m; (e) $x = 0.14$ m; and (f) $x = 0.15$ m.

Fig. 15 presents the axial load and its loss as the function of the axial displacement under different buckling configurations. From this figure, we can observe that when the axial displacement is less than 0.1 m, the axial forces at the loading and the dead ends increase linearly with the axial displacement. When the axial displacement is between 0.1 m and 0.14 m, the axial force at the dead end drops, even that the force at the loading end increases with the axial displacement. Once the axial displacement is greater than 0.14 m, the load changes at both ends are very nonlinear, which are reflected by the large fluctuations in the axial force loss. To refer to the buckling configurations in Fig. 14, point A, corresponding to Fig. 14(a), is the start point of the sinusoidal buckling, and the sinusoidal buckling is converted to the helical buckling completely at point B, which corresponds to Fig. 14(e). The loss of the axial load indicates the inefficiency of the axial load transfer once buckling is encountered. When the drill-string is straight, the loss of the axial load is small, and this loss is kept constant until sinusoidal buckling is encountered. Once the drill-strings is in helical buckling only, the trend of the axial load loss

becomes fluctuated as the axial displacement increases.

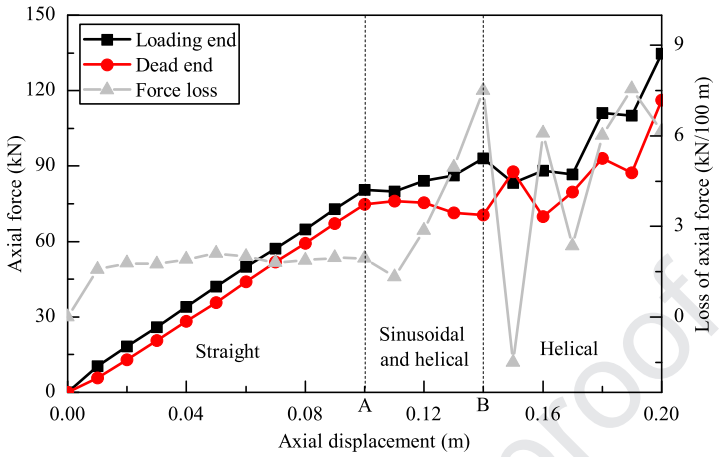

Figure 15: (Colour online) The axial loads at the loading (black squares) and the dead (red circles) ends and their loss (grey triangles) as a function of the axial displacement.

Fig. 16 demonstrates the distribution of the contact force along the drill-strings under different axial displacements shown in Fig. 14. As the displacement increases, the drill-strings and the casing have no contact before any buckling emerges at point A. Thereafter, contact forces are encountered along the drill-strings from the loading end to the dead end, and the entire drill-strings become helical buckling after point B.

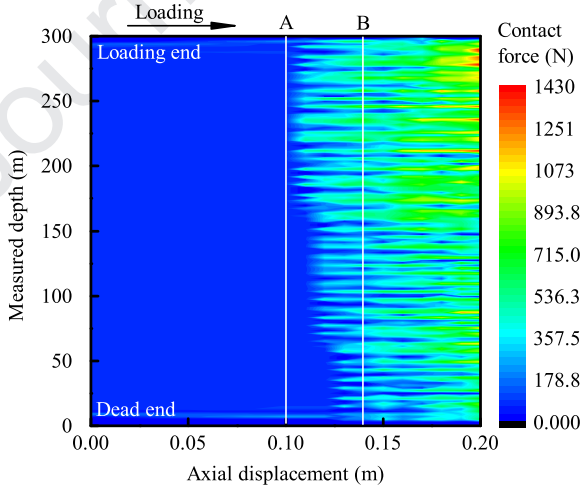

Figure 16: (Colour online) The map of the contact forces between the drill-strings and the casing calculated for a 300 m long drill-strings shown in Fig. 14. The drill-strings start to encounter buckling from point A, and become completely helical buckling from point B.

To study the influence of the friction coefficient between the string and the casing on the axial load transfer, calculations of the axial loads at both ends under different friction coefficients were presented in Fig. 17 as a function of the axial displacement. It can be seen from the figure, the axial loads at both ends increase linearly with the axial displacement until $x = 0.1$ m where an initial buckling is encountered. As the axial displacement increases, friction coefficient has more influence on both ends, since more buckling configurations emerge along the drill-strings. After the drill-strings are completely in helical buckling at $x = 0.14$ m, the axial load at the loading end is more sensitive to friction coefficient than the one at the

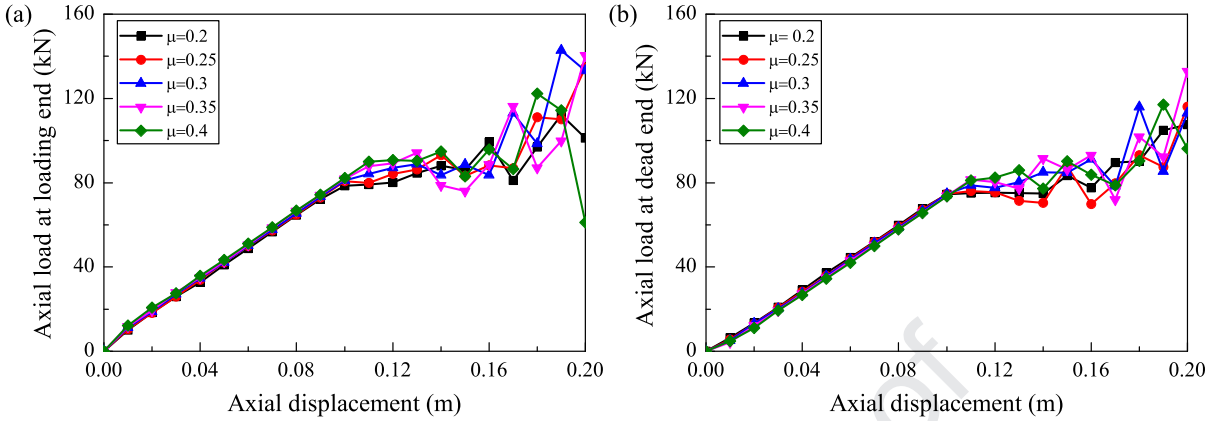

Figure 17: (Colour online) Axial load at (a) the loading end and (b) the dead end as a function of the axial displacement under different string-casing friction coefficients μ.

dead end.

5. Conclusions

This paper mainly studied the axial load transfer along the entire drill-strings in a deviated well by employing a finite element model taking into account the nonlinear pipe-casing contact and actual well trajectory. Based on this newly built model, our studies focused on the analysis of the axial load loss, the distribution of the pipe-casing contact force and the drill-string deformation, including both pulling-out and tripping-in operations. The efficacy of our proposed model was validated experimentally by using the field testing data obtained from a packer releasing procedure in an oil field. Through these analyses above, some useful conclusions and suggestions were obtained.

In pulling out operation, with the increase of hook load, the loss of axial load and the pipe-casing contact force are significantly increased in the build-up section, while have less variations in the inclined straight section. We studied the deviation angle and the overall angle change rate of the well trajectory. The results indicate that, the overall angle change rate has a significant effect on axial load transfer and constant force distribution. When this change rate remains constant, the loss of axial load increases linearly with the hook load. In addition, we found that the pulling-out axial force increases with the tripping velocity, and this effect is more obvious in the build-up section.

In horizontal well, with the increase of the axial displacement, both sinusoidal and helical buckling configurations were observed along the drill-strings, and these buckling configurations were transferred from the loading end to the dead end until the entire drill-strings became helical buckling. This causes the axial load transfer more sensitive to the string-casing friction coefficient, since the string-casing contact due to buckling degrades the efficiency of axial load transfer.

The FEM established in this paper, taking into account the actual well trajectory and nonlinear pipe-casing contact, provides an effective approach to prediction of the axial load transfer along the drill-strings in the deviated wells. Moreover, the theoretical guidance can be obtained to guide the parameter control in actual drilling.

Acknowledgements

Mr Wei Lin would like to acknowledge the financial support from the China Scholarship Council (Award no. 201708510133) for his one year visiting study at the University of Exeter.

References

Aadnoy, B., Andersen, K., 1998. Friction analysis for long-reach wells, in: IADC/SPE drilling conference, Society of Petroleum Engineers.

Adewuya, O.A., Pham, S.V., 1998. A robust torque and drag analysis approach for well planning and drillstring design, in: IADC/SPE drilling conference, Society of Petroleum Engineers.

Brett, J., Beckett, A., Holt, C., Smith, D., 1987. Uses and limitations of a drillstring tension and torque model to monitor hole conditions, in: SPE Annual Technical Conference and Exhibition, Society of Petroleum Engineers.

Cebeci, M., Kök, M.V., 2019. Analysis of sinusoidal buckling of drill string in vertical wells using finite element method, in: SPE Middle East Oil and Gas Show and Conference, Society of Petroleum Engineers.

Chen, Y., Fu, J., Ma, T., Tong, A., Guo, Z., Wang, X., 2018. Numerical modeling of dynamic behavior and steering ability of a bottom hole assembly with a bent-housing positive displacement motor under rotary drilling conditions. Energies 11, 1–23.

Duman, O.B., Miska, S., Kuru, E., 2003. Effect of tool joints on contact force and axial-force transfer in horizontal wellbores. SPE drilling & completion 18, 267–274.

Gao, G., Miska, S., 2010. Effects of friction on post-buckling behavior and axial load transfer in a horizontal well. SPE Journal 15, 1–104.

Hestenes, M.R., 1969. Multiplier and gradient methods. Journal of optimization theory and applications 4, 303–320.

Hill, T., Chandler, R., 1998. Field curves for critical buckling loads in curving wellbores, in: IADC/SPE drilling conference, Society of Petroleum Engineers.

Ho, H., 1988. An improved modeling program for computing the torque and drag in directional and deep wells, in: SPE Annual Technical Conference and Exhibition, Society of Petroleum Engineers.

Huang, W., Gao, D., 2019. Combined effects of wellbore curvature, connector, and friction force on tubular buckling behaviors. SPE Journal .

Johancsik, C., Friesen, D., Dawson, R., 1984. Torque and drag in directional wells-prediction and measurement. Journal of Petroleum Technology 36, 987–992.

Kapitaniak, M., Hamaneh, V.V., Chávez, J.P., Nandakumar, K., Wiercigroch, M., 2015. Unveiling complexity of drill–string vibrations: Experiments and modelling. International Journal of Mechanical Sciences 101, 324–337.

Kapitaniak, M., Hamaneh, V.V., Wiercigroch, M., 2016. Torsional vibrations of helically buckled drillstrings: experiments and FE modelling. Journal of Physics: Conference Series 721, 012012.

Kapitaniak, M., Vaziri, V., Wiercigroch, M., 2018a. Helical buckling of thin rods: FE modelling, in: MATEC Web of Conferences, EDP Sciences. p. 02010.

Kapitaniak, M., Vaziri, V., Wiercigroch, M., Manoach, E., Stoykov, S., Wiercigroch, M., 2018b. Helical buckling of drill-strings, in: MATEC Web of Conferences, EDP Sciences. p. 16007.

Kuang, Y., Li, B., Liu, J., Lu, H., 2016. Research on buckling behavior and analysis of sensitive factors in horizontal well drilling. Journal of Failure Analysis and Prevention 16, 376–383.

Leigh, E., Kunz, D.L., 2007. Simulation of a moving elastic beam using hamilton's weak principle. AIAA journal 45, 471–476.

Lubinski, A., 1950. A study of the buckling of rotary drilling strings, in: Drilling and Production Practice, American Petroleum Institute.

Lubinski, A., Althouse, W., 1962. Helical buckling of tubing sealed in packers. Journal of Petroleum Technology 14, 655–670.

Maehs, J., Renne, S., Logan, B., Diaz, N., 2010. Proven methods and techniques to reduce torque and drag in the pre-planning and drilling execution of oil and gas wells, in: IADC/SPE Drilling Conference and Exhibition, Society of Petroleum Engineers.

Meier, C., Popp, A., Wall, W.A., 2014. An objective 3d large deformation finite element formulation for geometrically exact curved kirchhoff rods. Computer Methods in Applied Mechanics and Engineering 278, 445–478.

Menand, S., Isambourg, P., Sellami, H., Simon, C., Bouguecha, A., 2009. Axial force transfer of buckled drill pipe in deviated wells, in: SPE/IADC Drilling Conference and Exhibition, Society of Petroleum Engineers.

Miller, J., Su, T., Pabon, J., Wicks, N., Bertoldi, K., Reis, P.M., 2015. Buckling of a thin elastic rod inside a horizontal cylindrical constraint. Extreme Mechanics Letters 3, 36–44.

Mirhajmohammadabadi, S.A.A., Fazaelizadeh, M., Kaarstad, E., Aadnoy, B.S., 2010. New aspects of torque-and-drag modeling in extended-reach wells, in: SPE Annual Technical Conference and Exhibition, Society of Petroleum Engineers.

Miska, S., Qiu, W., Volk, L., Cunha, J., 1996. An improved analysis of axial force along coiled tubing in inclined/horizontal wellbores, in: International conference on horizontal well technology, Society of Petroleum Engineers.

Mitchell, R., 1996. Comprehensive analysis of buckling with friction. SPE Drilling & Completion 11, 178–184.

Mitchell, R.F., Miska, S.Z., 2006. Helical buckling of pipe with connectors and torque. SPE Drilling & Completion 21, 108–115.

Omojuwa, E.O., Osisanya, S.O., Ahmed, R.M., 2012. Computation of axial load and torque distribution in tubulars used for extended-reach horizontal wells using a holistic design philosophy, in: Abu Dhabi International Petroleum Conference and Exhibition, Society of Petroleum Engineers.

Qin, X., Gao, D., Huang, W., 2019. Frictional buckling analyses of a slender rod constrained in a horizontal cylinder. European Journal of Mechanics-A/Solids 76, 70–79.

Sheppard, M., Wick, C., Burgess, T., 1987. Designing well paths to reduce drag and torque. SPE Drilling Engineering 2, 344–350.

Shooshtari, A., Khajavi, R., 2010. An efficient procedure to find shape functions and stiffness matrices of nonprismatic euler–bernoulli and timoshenko beam elements. European Journal of Mechanics-A/Solids 29, 826–836.

Simo, J., Laursen, T., 1992. An augmented lagrangian treatment of contact problems involving friction. Computers & Structures 42, 97–116.

Thompson, J.M.T., Silveira, M., Heijden, G.H.M.V.D., Wiercigroch, M., 2012. Helical post-buckling of a rod in a cylinder: With applications to drill-strings. Proceedings of the Royal Society A 468, 1591–1614.

Tikhonov, V.S., Safronov, A.I., 2008. Numerical simulation of the drillstring-in-hole dynamics at rotary drilling, in: 9th Biennial ASME Conference on Engineering Systems Design and Analysis, Haifa, Israel, Paper No. ESDA2008-59165.

Wheeler, J.D., 1970. Method for calculating forces produced by irregular waves. Journal of Petroleum Technology 22, 359–367.

Yastrebov, V.A., 2013. Numerical methods in contact mechanics. John Wiley & Sons.

Zhu, X., Li, B., Liu, Q., Chang, X., Li, L., Zhu, K., Xu, X., 2015. New analysis theory and method for drag and torque based on full-hole system dynamics in highly deviated well. Mathematical Problems in Engineering 2015.

Highlights

- The non-linear finite element method is proposed by taking into account the nonlinear contact and the actual well trajectory.
- A field test was carried out to verify the finite element method.
- Contact force distribution is introduced to study the axial load loss.
- The well trajectory factors and buckling configurations are studied.